

PointCNN++: Performant Convolution on Native Points

Lihan Li^{1*} Haofeng Zhong^{1*} Rui Bu² Mingchao Sun³
Wenzheng Chen^{1†} Baoquan Chen^{1†} Yangyan Li^{2†}

¹Peking University ²Ant Group ³AMAP

Abstract

Existing convolutional learning methods for 3D point cloud data are divided into two paradigms: point-based methods that preserve geometric precision but often face performance challenges, and voxel-based methods that achieve high efficiency through quantization at the cost of geometric fidelity. This loss of precision is a critical bottleneck for tasks such as point cloud registration. We propose PointCNN++, a novel architectural design that fundamentally mitigates this precision-performance trade-off. It **generalizes sparse convolution from voxels to points**, treating voxel-based convolution as a specialized, degraded case of our more general point-based convolution. First, we introduce a point-centric convolution where the receptive field is centered on the original, high-precision point coordinates. Second, to make this high-fidelity operation performant, we design a computational strategy that operates **natively** on points. We formulate the convolution on native points as a Matrix-Vector Multiplication and Reduction (MVMR) problem, for which we develop a dedicated, highly-optimized GPU kernel. Experiments demonstrate that PointCNN++ **uses an order of magnitude less memory and is several times faster** than representative point-based methods. Furthermore, when used as a simple replacement for the voxel-based backbones it generalizes, it **significantly improves point cloud registration accuracies while proving both more memory-efficient and faster**. PointCNN++ shows that preserving geometric detail and achieving high performance are not mutually exclusive, paving the way for a new class of 3D learning with high fidelity and efficiency.

Our code will be open sourced.

1. Introduction

The proliferation of 3D sensing technologies has established point clouds as a primary data modality in domains like autonomous driving [14, 19, 51], robotics [22, 25, 36, 59], and augmented reality [3, 34, 35, 47]. As a direct representation of world geometry, a point cloud’s value is intrinsically tied to its high-fidelity spatial information. This very characteristic—inherently sparse and irregular data—

however, creates a fundamental challenge for modern computational hardware [2, 21, 31, 32] and software [1, 20, 30, 33] that are heavily optimized for dense and regular data.

To address this challenge, the study of convolution on point clouds has developed two competing paradigms, each embodying a significant compromise. The most prevalent, the voxel-based approach (Figure 1 II), resolves the conflict by **forcefully restricting the convolution on voxel grids**. This approach firstly applies a *global voxelization* to quantize an entire continuous space of interest into a set of sparse voxels, from which sparse convolutional operators are applied. While the performance issue of such convolution has been substantially addressed by leveraging the sparse nature of the data, with representative work from O-CNN [45], SP-Conv [10], to MinkowskiEngine [6], the quantization is an inherently lossy sampling operation, resulting in impaired fine geometric details—representing high-frequency spatial signals. The act of the global voxelization in the beginning of the process establishes an a priori error floor determined by the voxel size, posing a critical bottleneck to tasks like high-precision registration that depend on sub-voxel feature uniqueness.

An alternative philosophy, the point-based paradigm, attempts to preserve the data’s integrity by a relatively more gentle, usually learned, transformation of irregular points into a regular dense tensors, from which the convolution is then applied. Such transform-then-convolve approach (Figure 1 III) is shown to be effective in harvesting the fidelity in point clouds, as shown in the notable representative work of PointCNN [24] and KPConv [43]. However, while the convolution on the dense tensor is indeed computationally efficient, **significant inefficiency arises in the transformation from irregular to regular itself**. Such transformation introduces extra computation, parameters to learn and significant memory access—a major source of inefficiency in point cloud related computation on GPUs [26, 41]. Moreover, the implementation of such point-based methods often involves frequent usage of padding operations, which often intensifies the inefficiency.

This paper posits that this prevailing trade-off should not be viewed as a permanent compromise, but rather as a conflict that can be mitigated through holistic computational design. We introduce PointCNN++ (Figure 1 IV), an architectural design that resolves this conflict by advancing a new

*Equal contribution.

†Corresponding authors.

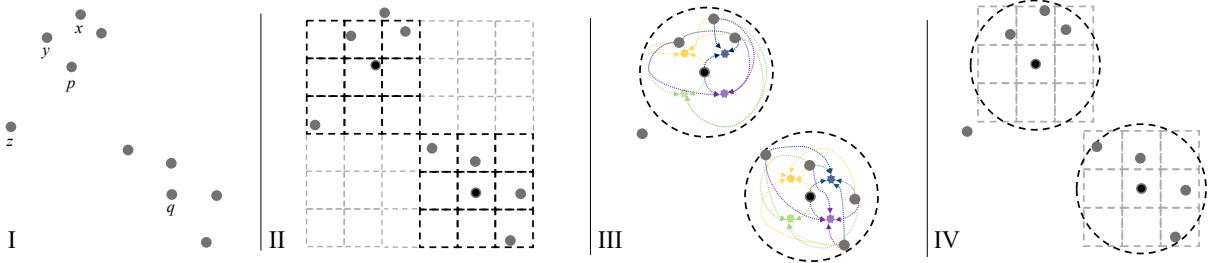


Figure 1. A 2D illustration of convolutional learning for point cloud (I) with voxel-based methods (II), transform-then-convolve methods (III) and convolution on native points (IV). When a voxel center happens to be on an original point (the rare case, as depicted by q), the difference between (II) and (IV) is minimal. However, in the general cases, due to the forceful restricting of computation on voxel grids in (II), several problems arise: 1. misalignment between original points (e.g., point p) and convolution centers, 2. inaccurate neighborhood inclusion (e.g., x , instead of z , should be in the neighborhood of p), and 3. inaccurate convolution kernel usage (e.g., the feature associated with point x is more appropriate for being convolved with the upper-left kernel as show in (IV), instead of the upper-middle kernel as shown in (II). IV preserves geometric precision as those in III, while avoiding the cumbersome irregular-to-regular “transformation”.

computational paradigm. Instead of **restricting the convolution** or **introducing extra transformation**, we design the operator and compute kernel as an integrated system, purpose-built for the high-performance processing of native point clouds, without any degradations nor superfluities. Our approach begins by generalizing sparse convolution from discrete voxels to continuous points, centering operations on the true, high-precision coordinates as much as possible. As the last operation, we use a *local and adaptive voxelization* to pair the data to be convolved with the discrete convolution kernels is used as the last operation to minimize the fidelity loss. From this perspective, voxel-based convolution is merely a quantized, degraded special case of our more fundamental point-centric operator. A more general operator, however, is only practical if it is performant. To this end, we formulate the convolution on native points as a Matrix-Vector Multiplication and Reduction (MVMR) problem. With this formulation, we drew inspiration from an efficient algorithm [40] for the Matrix-Vector Multiplication sub-problem to develop a dedicated, highly-optimized GPU kernel for the full problem.

In this paper, we introduce PointCNN++, an architectural design that mitigates the long-standing conflict between precision and performance in convolutional learning for 3D point cloud data. We empirically demonstrate that PointCNN++ not only excels on precision-critical tasks, but also is more memory-efficient while being even faster than existing approaches. This work proves that by holistically designing the computational system of point cloud data, achieving high geometric fidelity and high performance is not a mutually exclusive goal.

Our code will be open sourced.

2. Related Work

2.1. Feature Learning for 3D Point Cloud

Deep learning on point clouds has evolved through several operator paradigms. The seminal PointNet [37] processes each point independently with shared MLPs before global aggregation, while its successor PointNet++ [38] introduces

a hierarchical structure by recursively applying this process on nested point subsets. A central line of work focuses on generalizing convolution operator for 2D image data into processing 3D data. Voxel-based methods first discretize space for efficient 3D CNNs; for instance, VoxelNet [57] learns a unified feature representation for points within each voxel. PointCNN [24] proposes a learned \mathcal{X} -Transform to permute local point features into a canonical order before applying a convolution. PointConv [49] learns continuous kernel weights from relative coordinates using an MLP. KPConv [43] uses a set of rigid, learnable kernel points to apply spatially-aware weights. DGCNN [46] constructs dynamic graphs in feature space, and applies convolution on the feature space neighborhoods.

While Transformer has been widely used in processing 3D point cloud data, one thing to note is that they often operate on the features extracted with convolutional backbones [18, 23, 28, 29, 54, 55, 58], without which their effectiveness has not been widely demonstrated. Our work is most closely related to convolutional backbones in general, either used alone or as a part of a larger architecture, for serving general feature learning purposes on point cloud data. We show that with our systematic design, the performance advantage of the voxel-based methods and the precision advantage of point-based methods could be combined.

2.2. Performant Computation on Sparse Voxels

The performance of 3D deep learning is critically dependent on their underlying computational systems. The sparse nature of 3D data is extensively explored to efficiently process data while avoiding computation on empty space. SparseConvNet [13] pioneered the work in this domain, introducing the use of hashmaps to manage the coordinates of active voxels. Building on this, SpConv [50] proposed a highly-optimized grid-based map search and formalized the influential gather-matmul-scatter dataflow. MinkowskiEngine [6] significantly improved upon SparseConvNet’s hashmap implementation to reduce latency and introduced an alternative fetch-on-demand dataflow. More recent frameworks like TorchSparse [41] and TorchSparse++ [42] have continued to

push performance boundaries by developing novel traversal algorithms, hand-tuned CUDA kernels, and co-optimizing data structures and workloads specifically for GPU architectures. *fVDB* [48] integrated these concepts and further developed a flexible framework accepting various popular 3D data representations into the unified voxel-based representation upon which a rich set of operators is based. While existing high-performance methods typically exploit sparsity via voxelization, we show, however, that this is not a necessary coupling. Our approach achieves comparable computational efficiencies by leveraging sparsity directly on native point cloud representations, thereby bypassing the geometric precision loss inherent to voxelization.

3. Method

This section details the design principles of PointCNN++. Our methodology resolves the long-standing precision-performance dichotomy in 3D deep learning through a synergistic co-design of the core operator and its underlying computational system. We begin by establishing a generalized view of convolution and situating prior work within this framework in Sec. 3.1. We then introduce our point-centric convolution, highlighting its properties as a powerful generalization in Sec. 3.2. Finally, we describe the performant system design in Sec. 3.3, from the data representation to the optimized GPU kernel, that makes this high-fidelity operator computationally feasible at scale.

3.1. Preliminaries on Convolution

3.1.1. A Generalized View of Convolution

At its core, a convolution operator computes a feature $\mathbf{F}_i^{\text{out}} \in \mathbb{R}^{C_{\text{out}}}$ at location $\mathbf{P}_i^{\text{out}}$ by aggregating information from neighborhood locations $\{\mathbf{P}_j^{\text{in}}\}$, each associated with a feature $\mathbf{F}_j^{\text{in}} \in \mathbb{R}^{C_{\text{in}}}$, with the help of some learnable kernels $\{\mathbf{W}_k \in \mathbb{R}^{C_{\text{out}} \times C_{\text{in}}}\}$. C_{in} and C_{out} are dimensions, or channels, of the input and output features, respectively. The computational interactions among $\mathbf{F}_i^{\text{out}}$, \mathbf{F}_j^{in} , and \mathbf{W}_k , could be completely depicted by a triplet set $\mathcal{T} = \{(i, j, k)\}$, where a triplet (i, j, k) denotes that for convolution at location $\mathbf{P}_i^{\text{out}}$, location \mathbf{P}_j^{in} is in its neighborhood, and \mathbf{W}_k is the corresponding kernel to use for this neighborhood location. Thus, a generalized view of convolution could be formulated as:

$$\mathbf{F}_i^{\text{out}} = \sum_{(i,j,k) \in \mathcal{T}} \mathbf{W}_k \times \mathbf{F}_j^{\text{in}}. \quad (1)$$

The essence of different convolution types lies in how the triplet set $\mathcal{T} = \{(i, j, k)\}$ is constructed. More specifically, there are three major considerations in the construction of such triplets: ❶ How the locations of output features are placed? — Considerations on defining convolution centers $\{\mathbf{P}_i^{\text{out}}\}$ to use. ❷ How are the neighborhood measured? — Considerations on the pairing of $\{(i, j)\}$ in the triplet. ❸ Which kernel to use for a location in the neighborhood? — Considerations on the pairing of $\{(j, k)\}$ in the triplet.

3.1.2. Convolution on 2D Images

Convolution on 2D images is a specialized instance of Eqn. (1), where the triplet set $\{(i, j, k)\}$ is constructed by taking fully considerations on the dense and regular nature of the image data that is ubiquitously represented as discrete pixels: ❶ $\{\mathbf{P}_i^{\text{out}}\}$ are the pixels. ❷ $\{(i, j)\}$ are predefined as the pixels in patches around $\{\mathbf{P}_i^{\text{out}}\}$ are taken as neighborhoods, *i.e.*, Chebyshev distance based neighbors. ❸ For $\{(j, k)\}$, the kernels and neighborhoods are often of the same spatial resolution, thus $\{\mathbf{W}_k\}$ are paired with $\{\mathbf{P}_j^{\text{in}}\}$ if they share the same spatial locations.

Significant efforts have been made to achieve efficient GPU algorithms for the specialized triplet set \mathcal{T} of image convolution. In the early development stage of deep learning, image convolution was *not* a highly optimized standard operation on GPU. One way to achieve efficient computation was to materialize \mathbf{F}_j^{in} , thus lower the convolution into an highly optimized general matrix-matrix multiplication (GEMM), as practiced in the early version of Caffe [20]. However, as detailed in cuDNN [5], such materialization inevitably introduces significant amount of extra GPU memory usage, which could be addressed by lazily materializing in on-chip memory only.

3.1.3. Convolution on 3D Sparse Voxels

With a *global voxelization* of the entire 3D space of interest, often in the form of point cloud, the space could be sampled into sparse voxels — a representation that is a generalization of 2D pixels into 3D. By adding one dimension to the spatial coordinates, and relaxing the assumption of dense and regular tensor, convolution operator can be generalized from 2D images into 3D sparse voxels. Yet, convolution on 3D sparse voxels is still a specialized instance of Eqn. (1), as illustrated in Figure 1 II: ❶ $\{\mathbf{P}_i^{\text{out}}\}$ are the discrete voxels. ❷ $\{(i, j)\}$ are constructed by taking the non-empty voxels around $\{\mathbf{P}_i^{\text{out}}\}$ as neighborhoods, *i.e.*, again, Chebyshev distance based neighbors. ❸ Same as that in convolution on 2D images, $\{(j, k)\}$ are constructed by corresponding same spatial locations.

While efficient GPU algorithms of voxel-based convolution have been proposed in notable representative work from O-CNN [45], SPCConv [10], to MinkowskiEngine [7, 9]. There are inherent drawbacks arise from the definition of voxel-based convolution: (1) placing $\{\mathbf{P}_i^{\text{out}}\}$ at the discrete voxels is at the cost of sacrificing fidelity from the original point cloud; (2) neighborhood construction in Chebyshev distance with imprecise centers intensifies the fidelity erosion; (3) the fineness of kernels are coupled with the fineness of voxelization. A more detailed discussion, and addressing, of such drawbacks are given after the introduction of our method in the next section.

3.2. Convolution on Native Points

Definition. Our design philosophy is to fully harvest the fidelity in the input point cloud. As illustrated in Figure 1 IV, We start by ❶ placing the convolution locations right at the original high-precision points, thus $\{\mathbf{P}_i^{\text{out}} \in \mathbb{R}^3\}$ are true, continuous coordinates in our formulation. Then, ❷ the pair-

ing of $\{(i, j)\}$ could be constructed based on neighborhood search using the precise convolution centers with appropriate distance metrics on continuous space. Finally ③, for constructing $\{(j, k)\}$, a *local voxelization*, centered right at $\mathbf{P}_i^{\text{out}}$ of the same spatial resolution as the kernels is applied in each neighborhood region, yielding a correspondence between the kernels $\{\mathbf{W}_k\}$ and $\{\mathbf{P}_j^{\text{in}}\}$ in the neighborhood voxels.

Advantages. It is clear that both ① and ② operates on the full precision of the original point cloud, the quality of the neighborhood regions are well preserved. It is only at the final step, ③, with the convolution centers align exactly with neighborhood region centers, a *local voxelization* is applied. Such a local voxelization is adaptive to each neighborhood region, resulting in a higher quality mapping between $\{\mathbf{W}_k\}$ and $\{\mathbf{P}_j^{\text{in}}\}$. Note that, with given neighborhood regions, it is the appropriate fineness of the convolution kernels that defines the resolution of the local voxelization, rather than being coupled to the fineness of the global voxelization as that in convolution on sparse voxels.

Voxel Convolution as a Special Case. With the definition of convolution on native points, now we show that convolution on voxels is a special case of convolution on native points, by demonstrating the three degradations have to take that convert convolution on native points into convolution on voxels. First of all, such conversion inevitably introduce a global voxelization to generate voxels that are not necessary for convolution on the native points, but mandatory for convolution on voxels. Degradation ①, instead of using the original points as the convolution centers, snapping the convolution centers into the centers of the voxels. Degradation ②, instead of searching neighbors with the original points as centers within other points, searching neighbors in the voxel space. Degradation ③, instead of choosing appropriate fineness thus resolution of the kernels, using the resolution that is coupled to the size of receptive field in the global voxelized space.

For degradation ③, in other words, convolution on native points decouples kernel resolution from the receptive field’s physical span, whereas convolution on voxels couples it to the voxel resolution in the receptive field. We demonstrate the difference with some examples. In convolution on native points, given a neighborhood of points, kernels with fineness of either 3^3 or 5^3 could be used up to demand, as the continuous coordinates could result in any of the local voxels. In contrast, in convolution on voxels, if a neighborhood is constructed with 3^3 voxels based on the global voxelization, it does not make sense to use kernels of 5^3 resolution to convolve with such a neighborhood, as the neighborhood has been quantized into the coarser 3^3 voxels, leaving the extra fineness of 5^3 kernels useless.

3.3. Performant Systematic Design

The flexibility of convolution on native points presents a significant computational challenge. To make this high-fidelity design feasible at scale, we introduce a performant systematic design that spans from the fundamental computation abstraction to a highly-optimized GPU kernel.

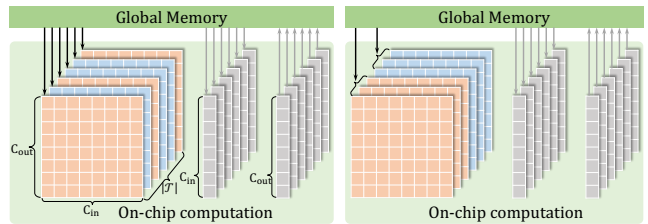


Figure 2. A brute-force MVM computation inefficiently reads $\mathbf{W}_k \in \mathbb{R}^{C_{\text{out}} \times C_{\text{in}}}$ from global memory $|\mathcal{T}|$ times—once for every triplet(left). Sorting the triplets by k optimizes this. Ideally, each unique \mathbf{W}_k is loaded just once into on-chip memory and reused for all its associated computations(right).

3.3.1. Computational Abstraction: MVMR

Same as convolution on 2D images, convolution on native points is an instance of Eqn. (1). A tempting strategy for efficient computation of it is to adapt the *im2col* like memory materialization technique once was used from image convolution, to lower the computation into a large GEMM problem. The extra memory usage introduced by materialization of the kernels is $K \times C_{\text{out}} \times C_{\text{in}}$, where K is the number of kernel matrices to use, and $K = t^3$ if a t resolution convolution kernel on each spatial axis is used. While extra memory usage for materializing the kernels are manageable, the materialization of neighborhoods would result in extra memory usage of $N_{\text{in}} \times K \times C_{\text{in}}$, where N_{in} is the size of the input point cloud, which is K times larger than the original data. Note that, the materialization of neighborhoods would “fill in” every neighborhood to a uniform maximum size with padding, causing a memory footprint increase far greater than that seen in image convolution and rendering the strategy impractical. Clearly, the strategy that was effective in convolution on 2D images is certainly not acceptable in convolution for native points in terms of extra memory usage, not to mention the latency introduced by the involved memory read and write.

Considering that point cloud is inherently irregular, to the best of our knowledge, there is no special structure to leverage for an alternative strategy in lowering the computation of convolution on native points into a single performant primitive. Inspired by the way cuDNN [5] addresses the extra memory usage problem and its effectiveness, we hypothesize that a computation abstraction that literally follows the general Eqn. (1) formulation has the potential of being performant while achieving zero extra memory usage.

We abstract the computation of Eqn. (1) as a Matrix-Vector Multiplication and Reduction (MVMR) problem, with the observation that MVMR naturally decomposes into two distinct components: the $\mathbf{W}_k \times \mathbf{F}_j^{\text{in}}$ component is a Matrix-Vector Multiplication(MVM), which itself is a popular operation with rich studies on achieving performant computation on GPUs, and the rest component is a Reduction — another example of cases with performant solutions. We develop a unified efficient GPU algorithm by taking inspirations from existing studies on the two sub-problems.

3.3.2. Efficient GPU Algorithm of MVMR

First of all, a native MVM implementation is required because MVMR involves many small MVM computations. Calling a standard library routine for each computation individually from an outer loop would incur prohibitive launch overhead. Second, while the amount of multiplication and addition is fixed, the key to a performant implementation of MVMR lies in optimizing memory access patterns. GPU performance is critically dependent on: a) data locality, *i.e.*, how much data is accessed from fast, on-chip resources versus the much slower, off-chip global memory. b) coalesced memory access, where threads within a hardware warp access contiguous memory locations to maximize bandwidth.

The output of the convolution is a feature tensor $\mathbf{F}^{\text{out}} \in \mathbb{R}^{N_{\text{out}} \times C_{\text{out}}}$, where N_{out} is the size of the output point cloud. It is computed from three inputs to the convolution operator: 1) the input feature tensor $\mathbf{F}^{\text{in}} \in \mathbb{R}^{N_{\text{in}} \times C_{\text{in}}}$; 2) the weight matrix $\mathbf{W} \in \mathbb{R}^{K \times C_{\text{out}} \times C_{\text{in}}}$; 3) the collection of triplets $\mathcal{T} = \{(i, j, k)\}$, constructed based on the convolution definition, where i, j and k are integers in range $[0, N_{\text{out}}]$, $[0, N_{\text{in}}]$, and $[0, K]$, respectively. The computational interactions among \mathbf{F}^{out} , \mathbf{W} and \mathbf{F}^{in} are completely depicted by the triplets \mathcal{T} . In most cases, $K \ll N_{\text{in}} \simeq N_{\text{out}} \ll |\mathcal{T}|$.

Note that the process of each triplet is independent of others, as long as the conflict on Reduction write to \mathbf{F}^{out} is governed by atomic primitive. Therefore, there is a straightforward parallelism strategy to accomplish the computation of all the triplets: let each thread handle the computation of one triplet. While this strategy seems ideal in terms of parallelism, significant amount of slow global memory access is involved, as illustrated in Figure 2 (left):

$$|\mathcal{T}| \times \left(\underbrace{C_{\text{out}} \times C_{\text{in}}}_{\text{Read from } \mathbf{W}} + \underbrace{C_{\text{in}}}_{\text{Read from } \mathbf{F}^{\text{in}}} + \underbrace{C_{\text{out}}}_{\text{Atomic Write to } \mathbf{F}^{\text{out}}} \right). \quad (2)$$

Clearly, the global memory read from \mathbf{W} is a bottleneck, and therefore, this access pattern must be addressed to improve performance. Mathematically, the final results are invariant to the processing order of the triplets¹, but a sorting of the triplets could significantly change the memory access patterns, as illustrated in Figure 2 (right). More specifically, given the triplet list $\mathcal{T} = \{(i, j, k)\}$ sorted by k , if it is split into consecutive groups of length L , based on Pigeonhole Principle, *most* of the groups contain triplets that share the same k value. More specifically, in the case of $K \ll |\mathcal{T}|$, a practical approximations of the expectation number of unique k in each group is $1 + \frac{L \times K}{|\mathcal{T}|}$ ², which approaches 1, when $L \times K \ll |\mathcal{T}|$. Due to this reason, when each of such group is processed together, *almost* only one global memory read of \mathbf{W} is required for each group, and

¹Practically, the results may vary with order due to numerical effects (*e.g.*, floating-point arithmetic).

²This is a classic problem that combines order statistics with a variant of the coupon collector's problem. The expected number of unique values in a single group is $1 + (L - 1) \left[\frac{K(1 - (1 - \frac{1}{K})^{|\mathcal{T}|}) - 1}{|\mathcal{T}| - 1} \right]$.

Algorithm 1 MVMR Kernel for Computing Eqn. (1)

Inputs: $\mathbf{W}, \mathbf{F}^{\text{in}}, \mathcal{T}^L$.
Output: \mathbf{F}^{out} .

```

1:  $(\tilde{i}, \tilde{j}, \tilde{k}) \leftarrow \mathcal{T}_0^L$  ▷ initialize with the first triplet.
2:  $\tilde{\mathbf{W}} \leftarrow \mathbf{W}_{\tilde{k}}, \tilde{\mathbf{F}}^{\text{in}} \leftarrow \mathbf{F}_{\tilde{j}}^{\text{in}}$  ▷ read from global memory.
3:  $\tilde{\mathbf{F}}^{\text{out}} \leftarrow \tilde{\mathbf{W}} \times \tilde{\mathbf{F}}^{\text{in}}$  ▷ fast on-chip computation.
4: for all  $(i, j, k)$  in  $\mathcal{T}_{[1, 2, \dots, L-1]}^L$  do
5:   if  $j \neq \tilde{j}$  then
6:      $\tilde{j} \leftarrow j, \tilde{\mathbf{F}}^{\text{in}} \leftarrow \mathbf{F}_j^{\text{in}}$  ▷ read only if necessary.
7:   end if
8:   if  $k \neq \tilde{k}$  then
9:      $\tilde{k} \leftarrow k, \tilde{\mathbf{W}} \leftarrow \mathbf{W}_{\tilde{k}}$  ▷ read only if necessary.
10:  end if
11:  if  $i \neq \tilde{i}$  then
12:    atomicAdd $(\tilde{\mathbf{F}}^{\text{out}}, \mathbf{F}_{\tilde{i}}^{\text{out}})$  ▷ only if necessary.
13:     $\tilde{i} \leftarrow i, \tilde{\mathbf{F}}^{\text{out}} \leftarrow \tilde{\mathbf{W}} \times \tilde{\mathbf{F}}^{\text{in}}$  ▷ on-chip, fast.
14:  else
15:     $\tilde{\mathbf{F}}^{\text{out}} \leftarrow \tilde{\mathbf{F}}^{\text{out}} + \tilde{\mathbf{W}} \times \tilde{\mathbf{F}}^{\text{in}}$  ▷ on-chip, fast.
16:  end if
17: end for
18: atomicAdd $(\tilde{\mathbf{F}}^{\text{out}}, \mathbf{F}_{\tilde{i}}^{\text{out}})$ 

```

the overall global memory access could be effectively reduce to $\mathcal{O}(\frac{1}{L})$ of that in Eqn. (2):

$$\frac{|\mathcal{T}|}{L} \times \left(\underbrace{C_{\text{out}} \times C_{\text{in}}}_{\text{Read from } \mathbf{W}} + \underbrace{L \times C_{\text{in}}}_{\text{Read from } \mathbf{F}^{\text{in}}} + \underbrace{L \times C_{\text{out}}}_{\text{Atomic Write to } \mathbf{F}^{\text{out}}} \right). \quad (3)$$

Beyond the option of sorting \mathcal{T} by k , there are two alternatives: sorting by i and sorting by j . Following the analysis of the saving introduced from sorting by k , they would result in saving read from \mathbf{F}^{in} and atomic write to \mathbf{F}^{out} , respectively. However, both of these savings are less effective, as: 1) the amount to load from \mathbf{F}^{in} or atomic write to \mathbf{F}^{out} is often orders of magnitude smaller than the read from \mathbf{W} ; 2) the expectation number of unique i and j in each group is $1 + \frac{L \times N_{\text{out}}}{|\mathcal{T}|}$ and $1 + \frac{L \times N_{\text{in}}}{|\mathcal{T}|}$, respectively, — not as ideal as the $1 + \frac{L \times K}{|\mathcal{T}|}$ in the sorting by k case, as $K \ll N_{\text{in}} \simeq N_{\text{out}}$. Our analysis coincides with our profiling, thus we choose to sort by k . Nevertheless, the above analysis is based on typical configurations, in terms of unknown configurations, an auto tuning mechanism could be used to select the index to be sorted by, before the massive executions.

While the strategy of grouped processing on the triplet list sorted by k is effective in addressing the critical data locality issue, a naive parallelism strategy by letting each thread handle the computation of one group is impractical as there is often not enough on-chip memory to afford an entire $C_{\text{out}} \times C_{\text{in}}$ matrix for each thread. We discern that the MVM sub-problem in MVMR is an extreme case of an already specialized Tall-and-Skinny Matrix-Matrix Multiplication problem, by viewing a vector as a one column matrix, for which an efficient GPU algorithm is proposed in [40]. We refer the readers to [40] for the design considerations and details that could be easily adopted into our MVM sub-problem. Heavily based on this, a practical and coalesced memory access friendly parallelism strategy that integrates the afore-

mentioned grouping logic is proposed. This strategy divides each of the $C_{\text{out}} \times C_{\text{in}}$ kernel matrix into $B_{\text{out}} \times B_{\text{in}}$ blocks, respectively, and assigns the computation related to each block of a group’s MVM computation to a warp of threads, rather than assigning the entire computation to a single thread.

We summarize our algorithm for efficient computation of MVMR in Algorithm 1, where $\mathcal{T}^L = \{(i, j, k)\}$ are the L triplets assigned to a warp of threads, and on-chip resources are denoted as $\tilde{\mathbf{W}} \in \mathbb{R}^{B_{\text{out}} \times B_{\text{in}}}$, $\tilde{\mathbf{F}}^{\text{in}} \in \mathbb{R}^{B_{\text{in}}}$, and $\tilde{\mathbf{F}}^{\text{out}} \in \mathbb{R}^{B_{\text{out}}}$. Note that effective global memory access saving are supported for all the three sorting options in Algorithm 1. An implementation based on Triton [44] is provided in supplementary materials. There are three hyperparameters in our algorithm, L , B_{out} and B_{in} , we use 128, 32 and 32, respectively, in all of our experiments.

Note that there is zero extra memory usage, as all the computation are native on the input tensors, without resorting to any intermediate global memory — an achieved goal similar to that in cuDNN [5] on the implementation of efficient convolution for dense and regular data. The one and only “extra” computation in our algorithm is the sorting of the triplets by k , which is an highly optimized parallel algorithm on GPU, the latency of which is negligible.

3.3.3. Efficient Gradient Computation

An efficient backward pass is critical for performant model training and finetuning. By applying the chain rule to our generalized convolution as described in Eqn. (1), two required gradients in distinct computational patterns are revealed, both of which demand efficient computation.

First, the gradient with respect to the input feature \mathbf{F}_j^{in} is an accumulation of transformed output gradients:

$$\nabla_{\mathbf{F}_j^{\text{in}}} \mathcal{L} = \sum_{(i,j,k) \in \mathcal{T}} \mathbf{W}_k^T \times \nabla_{\mathbf{F}_i^{\text{out}}} \mathcal{L}. \quad (4)$$

This operation mirrors the structure of the forward pass, where a set of matrices (now the transposed weights, \mathbf{W}_k^T) are multiplied by a set of vectors (the incoming gradients, $\nabla_{\mathbf{F}_i^{\text{out}}} \mathcal{L}$) and reduced. Consequently, this computation can be framed as an MVMR problem, allowing us to leverage the very same highly-optimized kernel designed for the forward pass, ensuring high efficiency.

Second, computing the gradient with respect to a weight kernel \mathbf{W}_k involves summing the outer products of the upstream output gradients and the corresponding input feature vectors over all associated triplets:

$$\nabla_{\mathbf{W}_k} \mathcal{L} = \sum_{(i,j,k) \in \mathcal{T}} \nabla_{\mathbf{F}_i^{\text{out}}} \mathcal{L} \otimes \mathbf{F}_j^{\text{in}}. \quad (5)$$

This structure follows a different pattern, which we abstract as Vector-Vector Outer product and Reduction (VVOR). For this, we develop a second dedicated GPU kernel, following similar principles used to develop the kernel for MVMR, which efficiently computes these outer products and reduces them into the final weight gradients. The algorithm details, as well as its Triton based implementation, of VVOR, are provided in the supplementary materials.

By implementing the backward pass with these two specialized, performant kernels—reusing MVMR for feature gradients and introducing VVOR for weight gradients—we ensure that the entire training process is computationally efficient, completing our holistic system design.

4. Experiments

Our experiments are designed to validate that PointCNN++ delivers both high performance and high fidelity. We first detail our implementation in Sec. 4.1, then use micro-benchmarks to quantify its GPU memory usage and computational efficiency with extensive comparisons against the performance prioritized voxel-based methods in Sec. 4.2, and finally demonstrate its accuracy on the geometrically sensitive task of point cloud registration in Sec. 4.3.

4.1. Implementation Details

We represent point clouds as jagged tensors same as that in [48], and also highlight specific architectural refinements. While not the core novelty of our work, these choices diverge from common practices and offer notable benefits for quality and robustness, which we hope will prove valuable to the community. We opt for a fixed radius search over a fixed-number (K-Nearest Neighbors, or KNN) search, as its spatially-local receptive field is better suited for convolutional learning, whereas KNN is often a choice imposed by architectural limitations. For sampling, we employ a voxel-based downsampling that, by not snapping points to voxel centers, better preserves thin structures and sparsely captured regions than random downsampling with negligible latency (contradicting the claim in [17] that random sampling is essential for efficiency), and we use the original pre-downsampled points for efficient upsampling. While these operations can be lowered into spatial lookups as in Open3D [56] with the underlying ASH [11] engine based on hash map, our empirical findings led us to implement a more robust and competitively fast mechanism built upon two highly-optimized GPU primitives: sorting and searching. The implementation of these operations will be open sourced alongside our core convolution operator.

4.2. Performance Study

This section is dedicated to analyzing the computational performance of our method. We establish its efficiency and scalability by benchmarking its memory footprint and latency against other representative methods on the isolated convolution operator level, as well as the timing for the end-to-end forward and backward passes³.

Experimental Setup. To ensure a fair and controlled comparison, all backbones used in this study are built upon a ResNet-18 [16] architecture. For the operator-level benchmarks, we use a standard convolution configuration ($C_{\text{in}} = 64, C_{\text{out}} = 128, K = 3^3$). We benchmark our method

³See supplementary material for performance benchmarks on various GPUs and scalability limits.

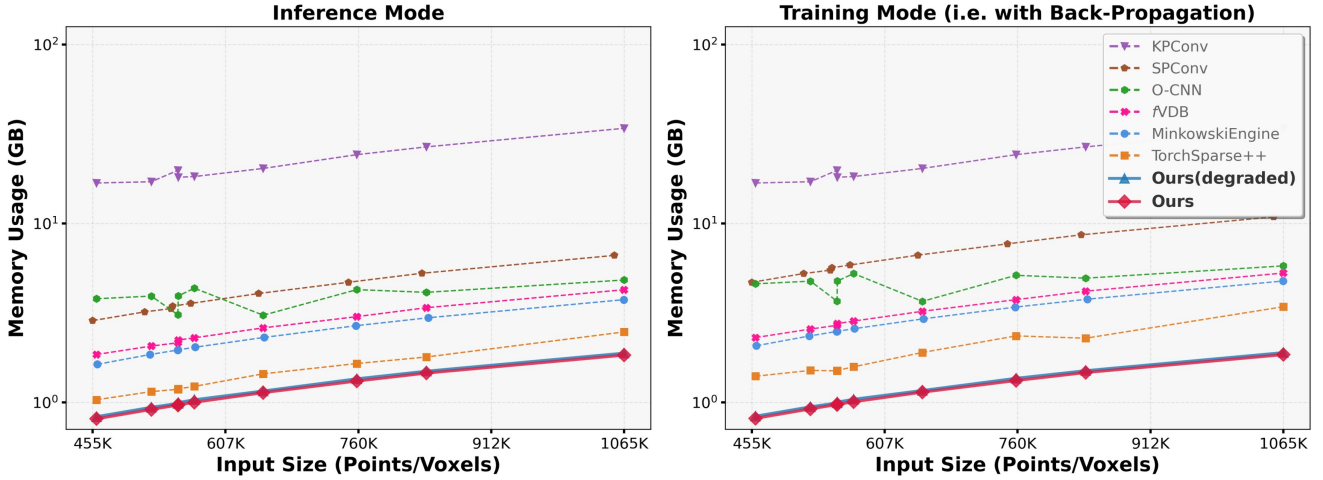


Figure 3. Memory usage comparison of one convolution layer.

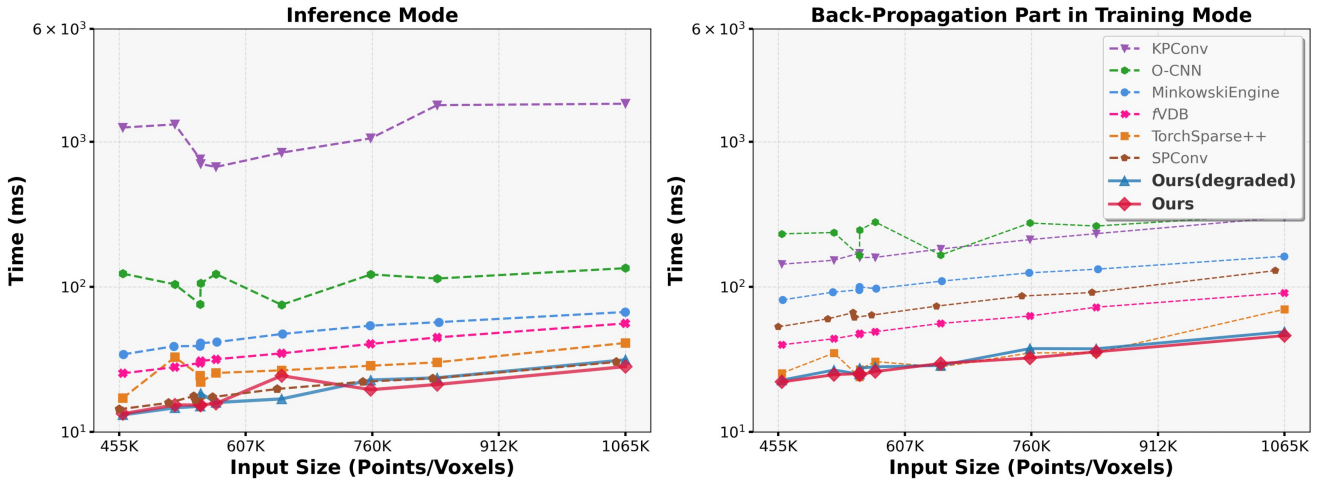


Figure 4. Performance comparison of one convolution layer.

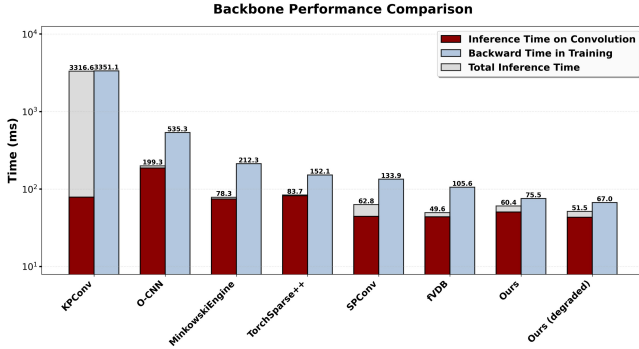
against several representative point-based [24, 43] and voxel-based [6, 10, 42, 45] backbones. Crucially, we also include a variant named ‘Ours (degraded)’, as described in Sec. 3.2. This allows us to directly quantify the performance difference between our approach and a traditional voxel-based paradigm within the same framework. For both latency and memory analysis, we use 10 large-scale scenes from the S3DIS dataset [4]. Timings and peak GPU memory consumption are recorded on a single NVIDIA RTX 4090 GPU. To ensure stability, all reported results are averaged over 10 independent runs per scene.

Memory Analysis. The results in Figure 5b highlight the superior memory efficiency of our operator. Across all tested resolutions, it consistently sets the lowest memory usage—less than half that of voxel-based methods such as MinkowskiEngine, TorchSparse++, and *fVDB*, and over an order of magnitude less than point-based baselines like KPConv. Although *fVDB* achieves strong voxel-level optimization and surpasses previous voxel methods, it still suffers from inherent overhead introduced by hierarchical data

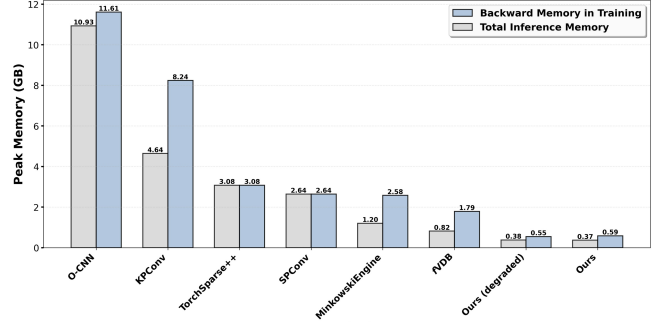
structures. In contrast, our point-native kernel design avoids any intermediate tensor materialization or padding, leading to an almost zero extra memory footprint during forward and backward propagation. Consequently, our method attains exceptionally low peak memory consumption (0.37GB for inference and 0.59GB for training), underscoring its intrinsic efficiency and scalability advantage.

Latency Analysis. Our analysis starts with the core convolution operator (Figure 4), where our method markedly outperforms leading point- and voxel-based alternatives. As shown in Figure 5a, the convolution operation dominates end-to-end runtime; thus, our operator-level advantage translates directly into superior overall performance.

While *fVDB* achieves highly optimized inference latency—comparable to our method—it lags significantly in back-propagation due to the overhead of traversing hierarchical voxel structures. In contrast, our co-designed MVVR and VVOR kernels enable efficient forward-backward coupling, yielding the lowest per-iteration time. As shown in Figure 5b, in the ResNet-18 benchmark, *fVDB* records a very



(a) Performance of various convolutional backbones for 3D learning assembled in an identical ResNet-18 [16] architecture.



(b) Memory usage of various convolutional backbones for 3D learning assembled in an identical ResNet-18 architecture.

Table 1. Quantitative comparison for point cloud registration on the KITTI. The best and second-best results are in red and blue. Architecture abbreviations: MkEngine (MinkowskiEngine), KP+Attn (KPConv with Attention), KP+GCN (KPConv with Graph Convolutional Network), and PNpp+Attn (PointNet++ with Attention), with task-specific designs of each method list in *italic*.

Method	Arch.	RTE(m) ↓		RRE(°) ↓		Recall(%) ↑ @0.2m,1°	Param
		Mean	Std	Mean	Std		
FCGF (2019)	MkEngine <i>ResUNet</i>	0.36	0.133	0.110	0.41	85.2	8.75M
DGR (2020)	MkEngine <i>IR prediction</i>	0.35	0.072	0.090	0.36	92.1	244.68M
CoFiNet (2021)	KP+Attn <i>Coarse2Fine</i>	0.39	0.065	0.091	0.39	89.4	5.48M
Predator (2021)	KP+GCN <i>Overlap pred.</i>	0.35	0.063	0.081	0.27	93.9	158.42M
GeoTrans (2022)	KP+Attn <i>Geom emb.</i>	0.38	0.068	0.096	0.29	85.6	25.50M
Regformer (2023)	PNpp+Attn <i>Prop-aware</i>	0.22	0.077	0.058	0.28	94.6	3.12M
UMEReg (2024)	MkEngine <i>UME + SEM</i>	0.49	0.023	0.490	0.21	79.6	7.17M
Ours (2025)	PointCNN++ <i>ResUNet</i>	0.19	0.03	0.060	0.10	99.8	8.75M

fast inference step (49.6 ms) but a slow backward pass (105.5 ms), whereas our method achieves a balanced profile with 60.4 ms for inference and only 75.5ms for back-propagation. This balance underscores PointCNN++’s superior efficiency in both inference and training.

Overall, our native point-centric operator matches the inference performance of optimized voxel frameworks like *f*VDB while surpassing them in total training efficiency, demonstrating clear architectural advantages for large-scale 3D learning. Interestingly, the voxel-based degraded variant of our method (Sec. 3.2) exhibits a slight speedup.⁴

4.3. Downstream Task: Point Cloud Registration

Our primary goal here is to investigate a simple yet critical question: *can solely replacing a standard voxel-based backbone with our geometrically faithful PointCNN++ counterpart yield significant performance gains?*

To this end, we deliberately avoid any task-specific tun-

⁴Although unexpected, we attribute this to a more cache-coherent access pattern centered on specific kernel regions, a hypothesis that warrants further study.

ing. We take the classic FCGF [7] architecture and simply replace its MinkowskiEngine-based backbone with our PointCNN++ implementation. All other components remain identical to the original FCGF. We then compare this straightforwardly upgraded model against a series of recent state-of-the-art methods, including DGR [8], Predator [18], CoFiNet [52], GeoTrans [39], Regformer [27], and UMEReg [15]. These methods often achieve high performance through highly-specific mechanisms and sophisticated designs.

In contrast, our approach brings only a better engine to a vintage chassis, yet, as we will show, proves to be remarkably competitive. Exploring the fusion of our backbone with advanced modules is left for future work.

We conduct evaluations on two standard benchmarks that represent distinct environments. KITTI Odometry [12] is a widely-used outdoor dataset from an autonomous driving platform, featuring sparse LiDAR scans. 3DMatch [53] is a large-scale indoor dataset composed of RGB-D scans from various scenes. Following UMEReg [15], we report Relative Translation Error (RTE), Relative Rotation Error (RRE) and Registration Recall (RR) on the KITTI. On the 3DMatch, we follow the protocol of CoFiNet [52] and use Registration Recall (RR), Feature Matching Recall (FMR), and Inlier Ratio (IR) for evaluation.

Results on KITTI. As shown in Table 1, the results on the KITTI dataset powerfully validate the effectiveness of our method in the zero-task specific tuning “plug-and-play” setting. By simply replacing the backbone in the classic FCGF architecture, we achieve state-of-the-art performance, nearly halving its RTE to 0.19m and boosting its RR to a near-perfect 99.8%. Beyond raw accuracy, our model demonstrates unparalleled registration stability, achieving the lowest standard deviations in both translation and rotation by a wide margin. This combination of top-tier accuracy and exceptional consistency proves that our high-fidelity operator produces superior features, leading to quantifiably better and more reliable registrations. The visualization in Figure 6 further illustrates the qualitative superiority of our method across different outdoor scenarios.

Results on 3DMatch. As shown in Table 2, our method demonstrates compelling results on the 3DMatch bench-

Table 2. Quantitative comparison on 3DMatch across different input point densities. We report Registration Recall (RR \uparrow), Feature Matching Recall (FMR \uparrow), and Inlier Ratio (IR \uparrow), all in percentages (%). The best results are in red bold, and the second best in blue bold.

Method	5000 Pts			2500 Pts			1000 Pts			500 Pts			250 Pts		
	RR	FMR	IR												
FCGF(2019)	85.1	97.4	52.8	84.7	97.3	51.1	83.3	97.0	46.7	81.6	96.7	41.5	71.4	96.6	34.1
CoFiNet(2021)	89.3	98.1	49.8	88.9	98.3	51.2	88.4	98.1	51.9	87.4	98.2	52.2	87.0	98.3	52.2
Predator(2021)	89.0	96.6	58.0	89.9	96.6	58.4	90.6	96.5	57.1	88.5	96.3	54.1	86.6	96.5	49.3
GeoTrans(2023)	91.4	97.9	70.5	91.1	98.0	72.9	92.0	98.1	75.2	91.7	98.2	79.8	91.2	98.3	84.6
Ours	90.3	98.9	58.2	90.2	99.1	57.8	89.2	99.1	57.3	89.1	98.4	52.1	88.3	99.2	53.4

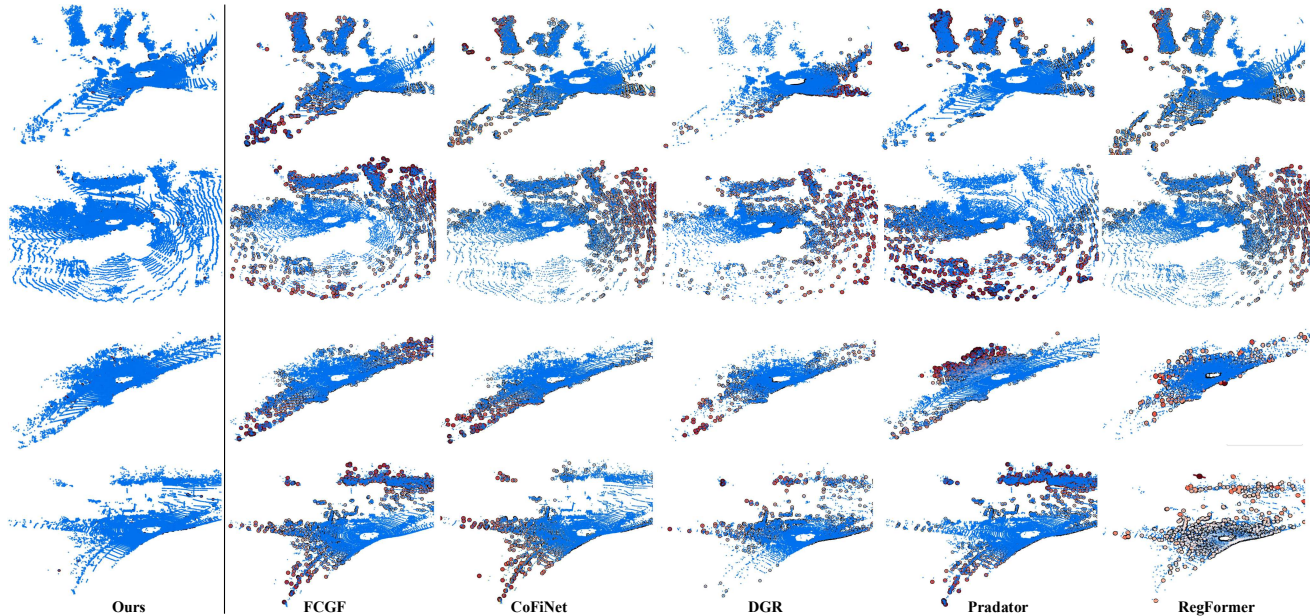


Figure 6. Point-wise registration error visualization on KITTI dataset comparing our method with state-of-the-art baselines.

mark. This is particularly noteworthy as these results are achieved using an old backbone, which is considerably simpler than the bespoke architectures of competitors like GeoTrans [39]. It indicates that our operator is powerful enough on its own to elevate a conventional architecture to produce features of state-of-the-art quality.

5. Conclusion

We present PointCNN++, a solution to the persistent trade-off in 3D deep learning between the performance of voxel-based grids and the precision of point-based operations. Our work dismantles this compromise by introducing a computational system designed specifically for irregular point clouds. By framing convolution on this data as an MVMR problem, we developed a dedicated GPU kernel that executes natively without the inefficient overheads. Our results confirm that sub-voxel accuracy could be retained without the performance penalties of prior methods, demonstrating that computational efficiency and geometric fidelity can be achieved in unison, enabling powerful, faithful geometric learning.

References

- [1] Martín Abadi, Paul Barham, Jianmin Chen, Zhifeng Chen, Andy Davis, Jeffrey Dean, Matthieu Devin, Sanjay Ghemawat, Geoffrey Irving, Michael Isard, et al. TensorFlow: a system for Large-Scale machine learning. In *12th USENIX symposium on operating systems design and implementation (OSDI 16)*, 2016.
- [2] Advanced Micro Devices (AMD). AMD CDNA 2 Architecture. Whitepaper, 2021. Available at: <https://www.amd.com/content/dam/amd/en/documents/instinct-business-docs/white-papers/amd-cdna2-white-paper.pdf>.
- [3] Evangelos Alexiou, Evgeniy Upenik, and Touradj Ebrahimi. Towards subjective quality assessment of point cloud imaging in augmented reality. In *2017 IEEE 19th international workshop on multimedia signal processing (MMSP)*, 2017.
- [4] Iro Armeni, Ozan Sener, Amir R Zamir, Helen Jiang, Ioannis Brilakis, Martin Fischer, and Silvio Savarese. 3d semantic parsing of large-scale indoor spaces. In *Proceedings of the IEEE conference on computer vision and pattern recognition*, 2016.
- [5] Sharan Chetlur, Cliff Woolley, Philippe Vandermersch, Jonathan Cohen, John Tran, Bryan Catanzaro, and Evan Shelhamer. cudnn: Efficient primitives for deep learning. *arXiv preprint arXiv:1410.0759*, 2014.

- [6] Christopher Choy, JunYoung Gwak, and Silvio Savarese. 4d spatio-temporal convnets: Minkowski convolutional neural networks. In *Proceedings of the IEEE Conference on Computer Vision and Pattern Recognition*, pages 3075–3084, 2019.
- [7] Christopher Choy, Jaesik Park, and Vladlen Koltun. Fully convolutional geometric features. In *Proceedings of the IEEE International Conference on Computer Vision*, pages 8958–8966, 2019.
- [8] Christopher Choy, Wei Dong, and Vladlen Koltun. Deep global registration. In *Proceedings of the IEEE/CVF conference on computer vision and pattern recognition*, 2020.
- [9] Christopher Choy, Junha Lee, Rene Ranftl, Jaesik Park, and Vladlen Koltun. High-dimensional convolutional networks for geometric pattern recognition. In *Proceedings of the IEEE Conference on Computer Vision and Pattern Recognition*, 2020.
- [10] Spconv Contributors. Spconv: Spatially sparse convolution library. <https://github.com/traveller59/spconv>, 2022.
- [11] Wei Dong, Yixing Lao, Michael Kaess, and Vladlen Koltun. ASH: A modern framework for parallel spatial hashing in 3d perception. *IEEE transactions on pattern analysis and machine intelligence*, 2022.
- [12] Andreas Geiger, Philip Lenz, and Raquel Urtasun. Are we ready for autonomous driving? the kitti vision benchmark suite. In *2012 IEEE conference on computer vision and pattern recognition*, 2012.
- [13] Benjamin Graham and Laurens Van der Maaten. Submanifold sparse convolutional networks. *arXiv preprint arXiv:1706.01307*, 2017.
- [14] An Guo, Yang Feng, and Zhenyu Chen. Lirtest: augmenting lidar point clouds for automated testing of autonomous driving systems. In *Proceedings of the 31st ACM SIGSOFT International Symposium on Software Testing and Analysis*, 2022.
- [15] Yuval Haitman, Amit Efraim, and Joseph M Francos. Umeregrobust-universal manifold embedding compatible features for robust point cloud registration. In *European Conference on Computer Vision*, 2024.
- [16] Kaiming He, Xiangyu Zhang, Shaoqing Ren, and Jian Sun. Deep residual learning for image recognition. In *Proceedings of the IEEE conference on computer vision and pattern recognition*, 2016.
- [17] Qingyong Hu, Bo Yang, Linhai Xie, Stefano Rosa, Yulan Guo, Zhihua Wang, Niki Trigoni, and Andrew Markham. Randla-net: Efficient semantic segmentation of large-scale point clouds. In *Proceedings of the IEEE/CVF conference on computer vision and pattern recognition*, 2020.
- [18] Shengyu Huang, Zan Gojic, Mikhail Usvyatsov, Andreas Wieser, and Konrad Schindler. Predator: Registration of 3d point clouds with low overlap. In *Proceedings of the IEEE/CVF Conference on computer vision and pattern recognition*, 2021.
- [19] Xinyu Huang, Xinjing Cheng, Qichuan Geng, Binbin Cao, Dingfu Zhou, Peng Wang, Yuanqing Lin, and Ruigang Yang. The apolloscape dataset for autonomous driving. In *Proceedings of the IEEE conference on computer vision and pattern recognition workshops*, 2018.
- [20] Yangqing Jia, Evan Shelhamer, Jeff Donahue, Sergey Karayev, Jonathan Long, Ross Girshick, Sergio Guadarrama, and Trevor Darrell. Caffe: Convolutional architecture for fast feature embedding. In *Proceedings of the 22nd ACM international conference on Multimedia*, 2014.
- [21] Norm Jouppi, George Kurian, Sheng Li, Peter Ma, Rahul Nagarajan, Lifeng Nai, Nishant Patil, Suvinay Subramanian, Andy Swing, Brian Towles, et al. Tpu v4: An optically reconfigurable supercomputer for machine learning with hardware support for embeddings. In *Proceedings of the 50th annual international symposium on computer architecture*, 2023.
- [22] Pileun Kim, Jingdao Chen, and Yong K Cho. Slam-driven robotic mapping and registration of 3d point clouds. *Automation in Construction*, 89:38–48, 2018.
- [23] Xin Lai, Jianhui Liu, Li Jiang, Liwei Wang, Hengshuang Zhao, Shu Liu, Xiaojuan Qi, and Jiaya Jia. Stratified transformer for 3d point cloud segmentation. In *Proceedings of the IEEE/CVF Conference on Computer Vision and Pattern Recognition*, pages 8500–8509, 2022.
- [24] Yangyan Li, Rui Bu, Mingchao Sun, Wei Wu, Xinhan Di, and Baoquan Chen. PointCNN: Convolution on \mathcal{X} -transformed points. *Advances in neural information processing systems*, 2018.
- [25] Jiong Lin, Lechen Zhang, Kwansoo Lee, Jialong Ning, Judah Goldfeder, and Hod Lipson. Autourdf: Unsupervised robot modeling from point cloud frames using cluster registration. In *Proceedings of the Computer Vision and Pattern Recognition Conference*, 2025.
- [26] Yujun Lin, Zhekai Zhang, Haotian Tang, Hanrui Wang, and Song Han. Pointacc: Efficient point cloud accelerator. In *MICRO-54: 54th Annual IEEE/ACM International Symposium on Microarchitecture*, 2021.
- [27] Jiuming Liu, Guangming Wang, Zhe Liu, Chaokang Jiang, Marc Pollefeys, and Hesheng Wang. Regformer: An efficient projection-aware transformer network for large-scale point cloud registration. In *Proceedings of the IEEE/CVF International Conference on Computer Vision*, 2023.
- [28] Zhijian Liu, Xinyu Yang, Haotian Tang, Shang Yang, and Song Han. Flatformer: Flattened window attention for efficient point cloud transformer, 2023.
- [29] Dening Lu, Qian Xie, Kyle Gao, Linlin Xu, and Jonathan Li. 3dctn: 3d convolution-transformer network for point cloud classification. *IEEE Transactions on Intelligent Transportation Systems*, pages 1–12, 2022.
- [30] John Nickolls, Ian Buck, Michael Garland, and Kevin Skadron. Scalable parallel programming with cuda: Is cuda the parallel programming model that application developers have been waiting for? *Queue*, 6(2):40–53, 2008.
- [31] NVIDIA. NVIDIA A100 Tensor Core GPU Architecture. Whitepaper, 2020. Available at: <https://www.nvidia.com/content/dam/en-zz/Solutions/Data-Center/nvidia-ampere-architecture-whitepaper.pdf>.
- [32] NVIDIA. NVIDIA H100 Tensor Core GPU Architecture. Whitepaper, 2022. Available at: <https://resources.nvidia.com/en-us-h100-whitepaper/h100-whitepaper-12-0922>.
- [33] Adam Paszke, Sam Gross, Francisco Massa, Adam Lerer, James Bradbury, Gregory Chanan, Trevor Killeen, Zeming Lin, Natalia Gimelshein, Luca Antiga, et al. Pytorch: An imperative style, high-performance deep learning library. In *Advances in Neural Information Processing Systems*, 2019.
- [34] Jette J Peek, Xucong Zhang, Klaus Hildebrandt, Samuel Alexander Max, Amir H Sadeghi, AJC Bogers,

- and EAF Mahtab. A novel 3d image registration technique for augmented reality vision in minimally invasive thoracoscopic pulmonary segmentectomy. *International journal of computer assisted radiology and surgery*, 20(4):787–795, 2025.
- [35] Alessio Pierluigi Placitelli and Luigi Gallo. Low-cost augmented reality systems via 3d point cloud sensors. In *2011 Seventh International Conference on Signal Image Technology & Internet-Based Systems*, 2011.
- [36] François Pomerleau, Francis Colas, Roland Siegwart, et al. A review of point cloud registration algorithms for mobile robotics. *Foundations and Trends® in Robotics*, 4(1):1–104, 2015.
- [37] Charles R Qi, Hao Su, Kaichun Mo, and Leonidas J Guibas. PointNet: Deep learning on point sets for 3d classification and segmentation. In *Proceedings of the IEEE conference on computer vision and pattern recognition*, 2017.
- [38] Charles Ruizhongtai Qi, Li Yi, Hao Su, and Leonidas J Guibas. PointNet++: Deep hierarchical feature learning on point sets in a metric space. *Advances in neural information processing systems*, 2017.
- [39] Zheng Qin, Hao Yu, Changjian Wang, Yulan Guo, Yuxing Peng, Slobodan Ilic, Dewen Hu, and Kai Xu. Geotransformer: Fast and robust point cloud registration with geometric transformer. *IEEE Transactions on Pattern Analysis and Machine Intelligence*, 2023.
- [40] Cody Rivera, Jieyang Chen, Nan Xiong, Jing Zhang, Shuaiwen Leon Song, and Dingwen Tao. Tsm2x: High-performance tall-and-skinny matrix–matrix multiplication on gpus. *Journal of Parallel and Distributed Computing*, 151: 70–85, 2021.
- [41] Haotian Tang, Zhijian Liu, Xiuyu Li, Yujun Lin, and Song Han. Torchsparse: Efficient point cloud inference engine. *Proceedings of Machine Learning and Systems*, 2022.
- [42] Haotian Tang, Shang Yang, Zhijian Liu, Ke Hong, Zhongming Yu, Xiuyu Li, Guohao Dai, Yu Wang, and Song Han. Torchsparse++: Efficient training and inference framework for sparse convolution on gpus. In *IEEE/ACM International Symposium on Microarchitecture (MICRO)*, 2023.
- [43] Hugues Thomas, Charles R Qi, Jean-Emmanuel Deschaud, Beatriz Marcotegui, François Goulette, and Leonidas J Guibas. KPConv: Flexible and deformable convolution for point clouds. In *Proceedings of the IEEE/CVF international conference on computer vision*, 2019.
- [44] Philippe Tillet, Hsiang-Tsung Kung, and David Cox. Triton: an intermediate language and compiler for tiled neural network computations. In *Proceedings of the 3rd ACM SIGPLAN International Workshop on Machine Learning and Programming Languages*, pages 10–19, 2019.
- [45] Peng-Shuai Wang, Yang Liu, Yu-Xiao Guo, Chun-Yu Sun, and Xin Tong. O-cnn: Octree-based convolutional neural networks for 3d shape analysis. *ACM Transactions On Graphics (TOG)*, 36(4):1–11, 2017.
- [46] Yue Wang, Yongbin Sun, Ziwei Liu, Sanjay E Sarma, Michael M Bronstein, and Justin M Solomon. Dynamic graph cnn for learning on point clouds. *ACM Transactions on Graphics (tog)*, 2019.
- [47] Zeyu Wang, Cuong Nguyen, Paul Asente, and Julie Dorsey. Pointshopar: Supporting environmental design prototyping using point cloud in augmented reality. In *Proceedings of the 2023 CHI conference on human factors in computing systems*, 2023.
- [48] Francis Williams, Jiahui Huang, Jonathan Swartz, Gergely Klar, Vijay Thakkar, Matthew Cong, Xuanchi Ren, Ruilong Li, Clement Fuji-Tsang, Sanja Fidler, et al. fvdb: A deep-learning framework for sparse, large scale, and high performance spatial intelligence. *ACM Transactions on Graphics (TOG)*, 2024.
- [49] Wenxuan Wu, Zhongang Qi, and Li Fuxin. Pointconv: Deep convolutional networks on 3d point clouds. In *Proceedings of the IEEE/CVF Conference on computer vision and pattern recognition*, 2019.
- [50] Yan Yan, Yuxing Mao, and Bo Li. Second: Sparsely embedded convolutional detection. *Sensors*, 2018.
- [51] Zetong Yang, Li Chen, Yanan Sun, and Hongyang Li. Visual point cloud forecasting enables scalable autonomous driving. In *Proceedings of the IEEE/CVF Conference on Computer Vision and Pattern Recognition*, 2024.
- [52] Hao Yu, Fu Li, Mahdi Saleh, Benjamin Busam, and Slobodan Ilic. Cofinet: Reliable coarse-to-fine correspondences for robust pointcloud registration. *Advances in Neural Information Processing Systems*, 2021.
- [53] Andy Zeng, Shuran Song, Matthias Nießner, Matthew Fisher, Jianxiong Xiao, and Thomas Funkhouser. 3dmatch: Learning local geometric descriptors from rgb-d reconstructions. In *Proceedings of the IEEE conference on computer vision and pattern recognition*, 2017.
- [54] Cheng Zhang, Haocheng Wan, Shengqiang Liu, Xinyi Shen, and Zizhao Wu. Pvt: Point-voxel transformer for 3d deep learning. *arXiv preprint arXiv:2108.06076*, 2021.
- [55] Hengshuang Zhao, Li Jiang, Jiaya Jia, Philip HS Torr, and Vladlen Koltun. Point transformer. In *Proceedings of the IEEE/CVF international conference on computer vision*, 2021.
- [56] Qian-Yi Zhou, Jaesik Park, and Vladlen Koltun. Open3D: A modern library for 3d data processing. *arXiv preprint arXiv:1801.09847*, 2018.
- [57] Yin Zhou and Oncel Tuzel. Voxelnet: End-to-end learning for point cloud based 3d object detection. In *Proceedings of the IEEE conference on computer vision and pattern recognition*, 2018.
- [58] Zixiang Zhou, Xiangchen Zhao, Yu Wang, Panqu Wang, and Hassan Foroosh. Centerformer: Center-based transformer for 3d object detection. In *ECCV*, 2022.
- [59] Haoyi Zhu, Yating Wang, Di Huang, Weicai Ye, Wanli Ouyang, and Tong He. Point cloud matters: Rethinking the impact of different observation spaces on robot learning. *Advances in Neural Information Processing Systems*, 2024.

PointCNN++: Performant Convolution on Native Points

Supplementary Material

This supplementary material provides additional details, benchmarks, and implementation specifics to support the claims made in the main paper. In Sec. F, we expand on the performance benchmarks culminating in a scalability analysis that stress-tests each method to its out-of-memory limit. For the point cloud registration task, Sec. G details the experimental protocols, datasets, and evaluation metrics, and presents extensive qualitative results that visually corroborate the quantitative superiority of our method. Finally, to ensure full transparency and reproducibility, Sec. H offers a deep dive into our custom GPU kernels, providing algorithmic pseudocode for our novel VVOR kernel and the complete Triton code for both the MVMR and VVOR implementations.

F. Extended Performance Analysis

This section provides additional benchmarks and details that complement the performance study in the main paper, further demonstrating the efficiency and scalability of our operator.

F.1. Full Benchmark Results

This section expands upon the performance benchmarks presented in the main paper (Figures 3, 4, 5, 6 in the main paper) to provide a more comprehensive analysis. For complete transparency and reproducibility, implementation details for all benchmarked methods are provided in Table C.

Table C. Implementation details for all benchmarked methods.

Method	Version
KPConv	-
SPConv	v2.3.8
O-CNN	v2.2.7
MinkowskiEngine	v0.5.4
TorchSparse++	v2.1.0
<i>f</i> VDB	v0.3.1
PointCNN	-
Ours (degraded)	-
Ours	-

F.2. Cross-GPU Performance Validation

To demonstrate that the performance advantages of our operator are not limited to a single GPU architecture, we conducted a rigorous cross-GPU performance validation. In addition to the RTX 4090 (Ada Lovelace architecture) benchmarks presented in the main paper, we tested a single convolution layer on three distinct NVIDIA data-center and professional GPUs: the A800 (Ampere), L20 (Ada Lovelace), and V100 (Volta). The latency results for both inference and training are presented in Figure G, Figure H, and Figure I. The findings are unequivocal: across every tested hardware platform, our method (Ours) consistently achieves the lowest latency for both forward and backward passes at all point cloud scales. This sustained leadership, from older architectures like Volta to the latest Ada Lovelace, provides strong evidence that the efficiency of our custom kernels is fundamental.

The performance gains are rooted in our co-designed, memory-centric computational strategy, rather than being an artifact of specific hardware features like L2 cache size or Tensor Core capabilities on a particular GPU. This demonstrates the robustness, generalizability, and broad applicability of PointCNN++ as a high-performance solution across a wide range of deployment scenarios and hardware platforms.

F.3. Scalability Limit Analysis

To quantify the memory scalability of different backbones, we conducted an end-to-end benchmark using an identical ResNet-18 architecture on point clouds of increasing size. Figure J plots the peak memory consumption for both the forward (inference) and backward (training) passes on a log-log scale. The results unequivocally demonstrate the superior memory efficiency of our native point-based approach (PointCNN++). The practical implications of these results are profound, as shown by the horizontal lines indicating common GPU memory capacities. During training (right plot), which is the most memory-intensive scenario, baseline methods hit hardware limits very quickly. In stark contrast, PointCNN++ comfortably processes point clouds up to ~ 100 M points on the same GPU, more than doubling the capacity of the next best method.

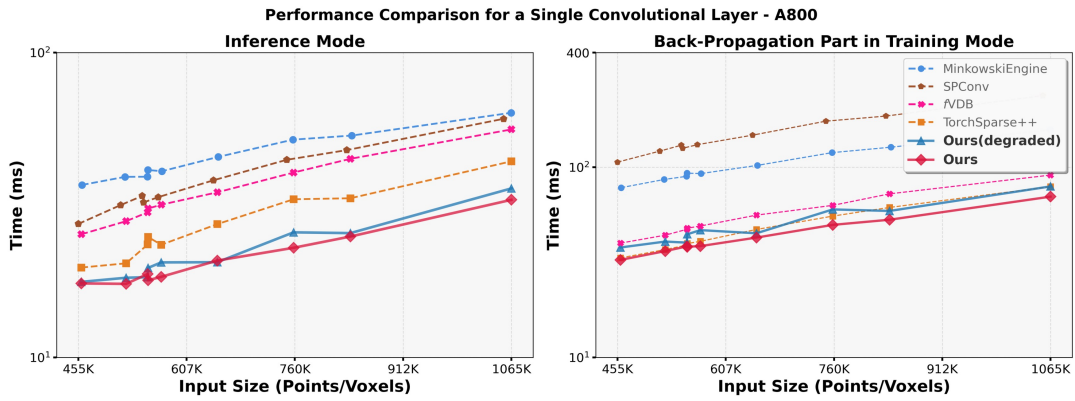


Figure G. Performance comparison of one convolution layer on A800.

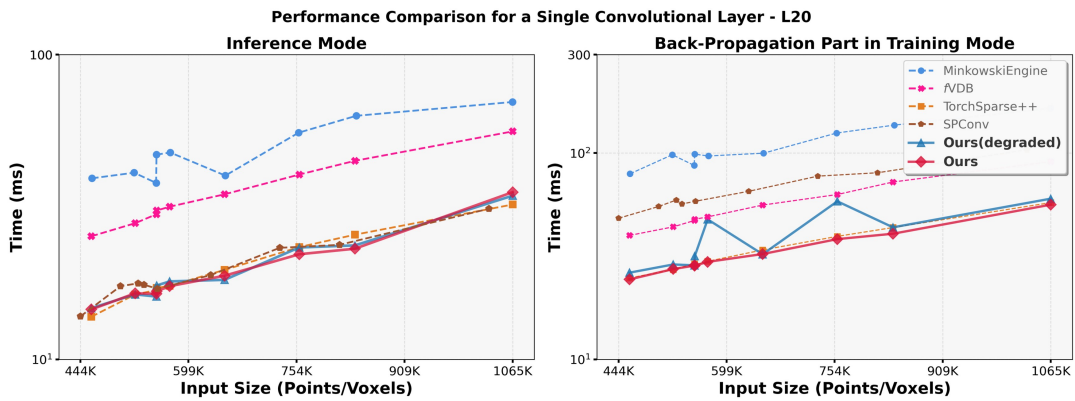


Figure H. Performance comparison of one convolution layer on L20.

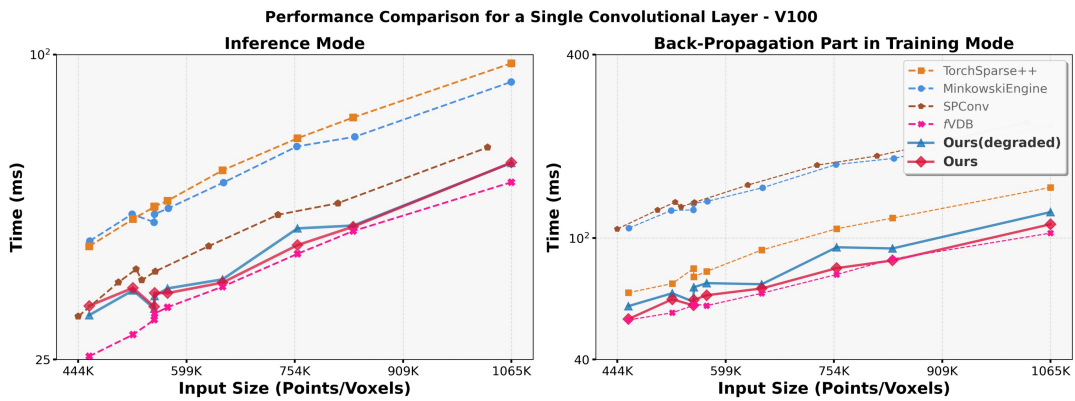


Figure I. Performance comparison of one convolution layer on V100.

This significant scalability disparity stems from fundamental design choices. Voxel-based methods (MinkowskiEngine, SPCConv, *fVDB*) and point-based methods (KPCConv) all rely on auxiliary data structures—such as hash maps or neighborhood graphs—that incur substantial and often non-linearly growing memory overhead. Our native approach, by directly operating on sorted point data with zero intermediate memory footprint, fundamentally circumvents this bottleneck. This exceptional memory efficiency makes PointCNN++ not just a faster alternative, but often the only feasible solution for training deep models on large-scale, real-world point clouds using standard hardware.

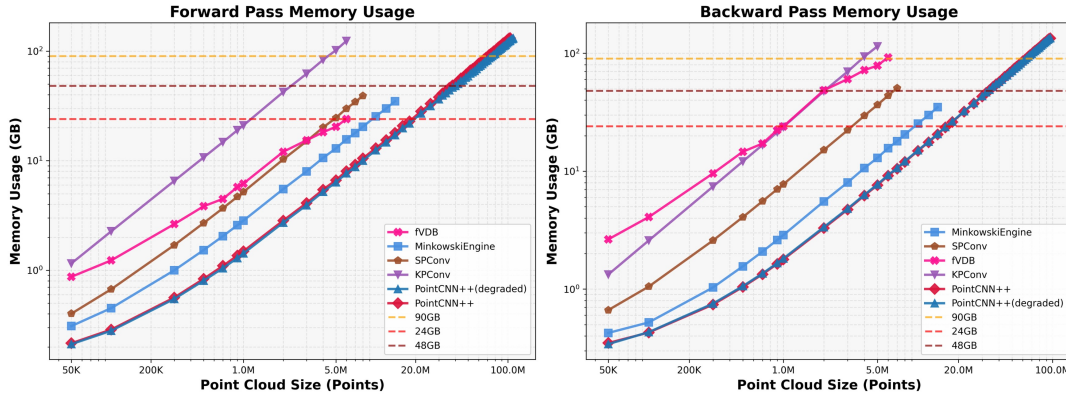


Figure J. Peak memory consumption of various ResNet-18 [16] backbones on point clouds of increasing size.

G. Additional Details on Point Cloud Registration

This section provides implementation details and qualitative results for the point cloud registration task discussed in the main paper.

G.1. Experimental Setup and Metric Definitions

G.1.1. Outdoor Scene Registration: KITTI Odometry

Dataset and Protocol. We follow the setup from GeoTransformer [39] for evaluation on the KITTI Odometry dataset [12]. Sequences 00-05 are used for training, 06-07 for validation, and 08-10 for testing. Following standard practice, the ground-truth poses are refined using ICP.

Evaluation Metrics. Following prior works [15, 39], we report three standard metrics for outdoor registration: **Evaluation Metrics.** Following prior works, we report three standard metrics for outdoor registration:

- Relative Rotation Error (RRE): The geodesic distance between the estimated and ground-truth rotation matrices, measured in degrees ($^{\circ}$).
- Relative Translation Error (RTE): The Euclidean distance between the estimated and ground-truth translation vectors, measured in meters (m).
- Registration Recall (RR): The fraction of test pairs that are successfully registered, defined as satisfying both $RRE < 1^{\circ}$ and root-mean-square error (RMSE) below 0.2m.

Baseline Comparison. On KITTI, in addition to RANSAC-based methods like FCGF, Predator, and GeoTransformer, we also compare against recent end-to-end registration methods such as DGR [8], Reformer [27], and UMEReg [15]. Strictly speaking, a direct comparison with RANSAC-based methods is sufficient to validate the feature quality of our backbone. However, our method’s performance on KITTI not only surpasses these feature-matching baselines but also exceeds that of several recent end-to-end solutions. Therefore, we include them to showcase the versatility and high potential of PointCNN++ as a powerful backbone applicable across different registration paradigms.

G.1.2. Indoor Scene Registration: 3DMatch

Dataset and Protocol. We follow the experimental setup of Predator [18] and evaluate on the 3DMatch dataset [53]. This dataset consists of 62 indoor scenes captured with RGB-D sensors, with a standard split of 46 scenes for training, 8 for validation, and 8 for testing. To ensure a fair comparison, we adhere to the same preprocessing pipeline and data splits used in the official public code of our baselines.

Evaluation Metrics. Following GeoTransformer [39], we evaluate the quality of feature matching with three metrics:

- Inlier Ratio (IR): The fraction of putative correspondences whose registration error is below a threshold ($0.1m$) under the ground-truth transformation.
- Feature Matching Recall (FMR): The fraction of point cloud pairs for which the inlier ratio is above a certain threshold (5%).
- Registration Recall (RR): The fraction of point cloud pairs that can be successfully registered, defined as achieving a correspondence root-mean-square error (RMSE) below $0.2m$ after pose estimation.

Baseline Comparison. On 3DMatch, we focus our comparison on RANSAC-based feature matching methods, including FCGF [7], CoFiNet [52], Predator [18], and GeoTransformer [39]. The performance of all methods is evaluated using the same RANSAC solver to ensure that the results are directly comparable. Unlike end-to-end regression or direct pose prediction methods, our primary goal here is to validate the improvement in feature representation brought by using PointCNN++ as a

backbone. This approach isolates the feature extraction stage, ensuring that performance gains are directly attributable to the quality of the learned descriptors rather than differences in pose regression model architectures.

Details on the #Samples Hyperparameter. Following the evaluation protocol of GeoTransformer [39], we also assess robustness by varying the number of correspondences used for RANSAC ($\#Samples \in \{5000, 2500, 1000, 500, 250\}$). The #Samples parameter refers to the maximum number of putative correspondences randomly sampled from the full set of matches. These samples are then fed into the RANSAC solver. This test evaluates the stability and robustness of the feature descriptors under varying correspondence densities: a large sample size represents an ideal scenario with ample matches, while a smaller sample size tests the method’s performance in sparse matching conditions.

G.1.3. RANSAC Configuration

For all methods employing a RANSAC-based solver (all methods on 3DMatch, and the feature-matching baselines on KITTI), we use a unified configuration to ensure a fair comparison of the underlying features. Specifically, we run 50,000 iterations of RANSAC to estimate the final rigid transformation. This standardized pose-solving procedure, consistent with the protocol in GeoTransformer [39], allows the final registration accuracy to directly reflect the quality of the feature descriptors provided by each backbone.

G.2. Qualitative Results on 3DMatch

As shown in Figure K, the results from our method (leftmost column) demonstrate a consistently superior alignment across all examples. The transformed source clouds (yellow) overlap tightly with the target clouds (blue), showing only very few and sparse red points, which indicates a highly accurate and robust registration with minimal error. In contrast, baseline methods exhibit visibly larger discrepancies. FCGF and CoFiNet, in particular, struggle on these challenging pairs, producing significant misalignments characterized by large, dense clusters of bright red points that suggest substantial errors in the estimated poses. Even stronger baselines like GeoTransformer and Predator, while achieving more plausible global alignments, still display more noticeable and larger patches of red points compared to our method, especially along planar surfaces and detailed structures. This indicates a lower level of precision in their fine-grained alignment. Overall, these qualitative results strongly corroborate our quantitative findings (Table 2 in the main paper), visually confirming that the superior feature representation learned by the PointCNN++ backbone enables our registration pipeline to achieve a more precise and reliable alignment than existing state-of-the-art methods.

H. Kernel Implementation Details

This section delves into the low-level implementation of our custom GPU kernels, providing pseudocode and code snippets for full transparency and reproducibility.

H.1. Efficient GPU Algorithm of VVOR

The backward pass requires computing the gradient with respect to the weight kernels \mathbf{W} . As defined in Eqn. (5) of the main paper, this involves summing the outer products of the upstream output gradients and the corresponding input feature vectors. We abstract this operation as Vector-Vector Outer-product and Reduction (VVOR).

Following the same design principles as our forward-pass MVMR kernel, we develop a second dedicated, highly-optimized GPU kernel for VVOR. It also operates on a list of triplets \mathcal{T} , and following a similar reasoning as that in computing MVMR, sorting the triplets by the kernel index k significantly saves *atomicAdd* operation for the relatively large kernel matrices, thus is preferred in typical configurations. The kernel leverages on-chip memory to accumulate the outer product results for each weight matrix \mathbf{W}_k , writing the final accumulated gradient matrix back to global memory only when the computation for that specific kernel is complete. This strategy minimizes costly global memory writes and achieves zero intermediate memory footprint. The algorithm for our VVOR kernel, which computes the gradient $\nabla_{\mathbf{W}}$, is detailed in Algorithm B.

H.2. Triton Code Implementation

To demonstrate the practical application of our proposed computational strategies, we provide implementations of the MVMR and VVOR kernels using Triton. Triton is a Python-based language and compiler for writing highly efficient GPU kernels. These listings map the high-level logic described in Algorithm 1 (in the main paper) and Algorithm B into Triton’s programming model, showcasing how on-chip accumulation and optimized memory access patterns are realized in practice.

Listing 1 presents the implementation of the MVMR kernel (*sparse_matrix_vector_multiplication_reduction_kernel*). As detailed in the main paper, this single, highly-optimized kernel is versatile, executing not only the forward pass but also the computation of input feature gradients $\nabla \mathbf{F}^{\text{in}}$ during the backward pass. This reuse is highly efficient as both operations reduce to the same MVMR computational pattern. The kernel processes a block of triplets, performs the corresponding matrix-vector products, and accumulates the results for each output point before writing them back to global memory via atomic operations.

Due to the reason that the kernel is used for both the forward and backward pass, thus the naming of the variables are not aligned with the notations in the forward pass nor those in the backward pass. Essentially, variable a and b indicate the inputs,

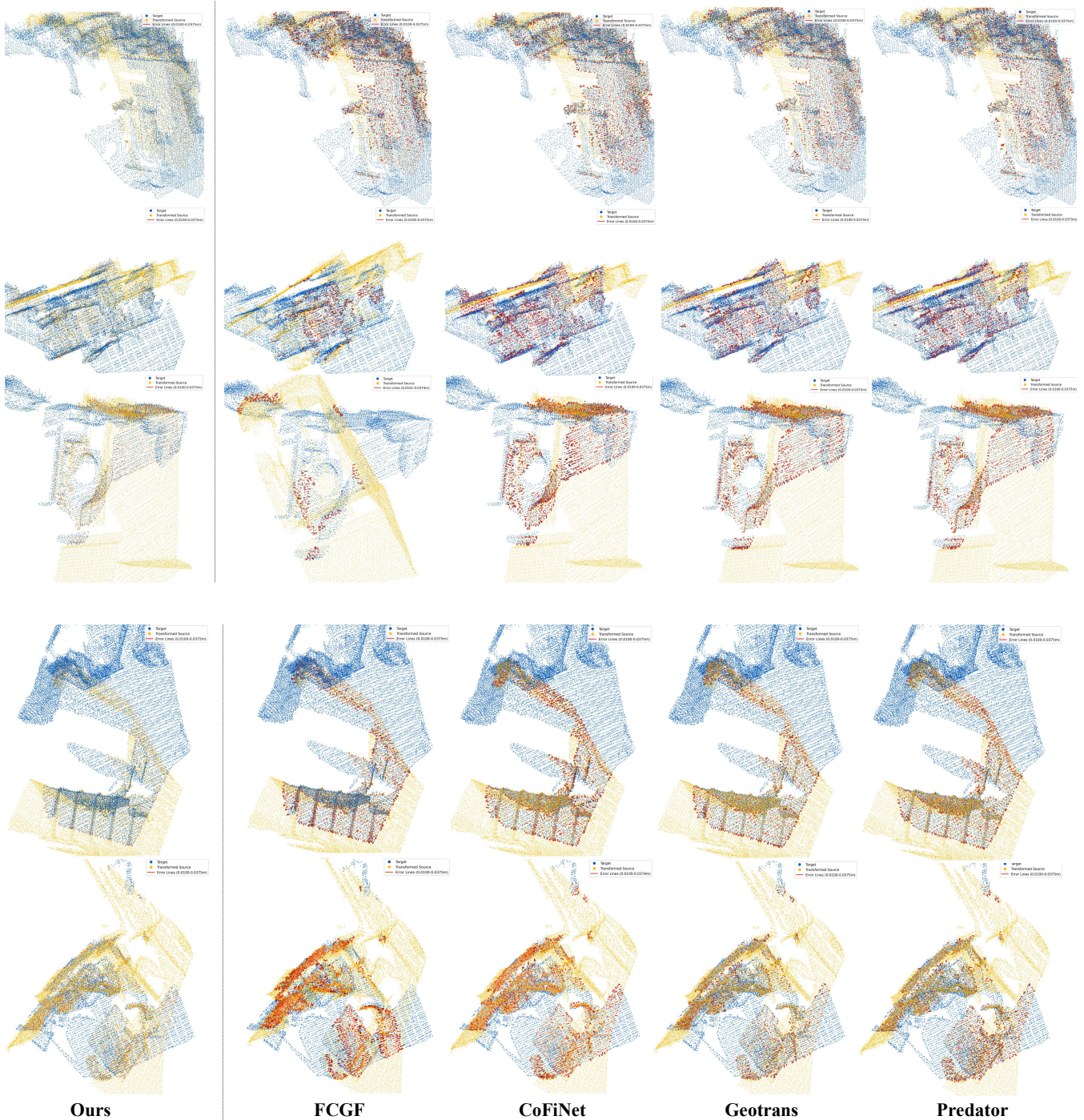


Figure K. Qualitative comparison on the 3DMatch [53] dataset.

while o is the output, and variables end with $_{idx}$ are the corresponding index. The variables T , M , and C corresponding the $|\mathcal{T}|$, C_{out} and C_{in} , respectively. Our code supports the widely used group convolution, and the variable G is the number of groups. Such naming scheme is used in all of our code.

Listing 2 shows the implementation of the VVOR kernel (`sparse_vector_vector_outer_product_reduction_kernel`), used for computing weight gradients in the backward pass. Here, the core operation is the outer product between the upstream gradient vector and the input feature vector. The results are accumulated on-chip into a gradient matrix, which is then atomically added to the corresponding global weight gradient matrix.

Note that while sorting triplets by k is typically the optimal choice, the support for sorting by i or j is also provided in our algorithm and code, as they share very similar logic. The PyTorch code for invoking the Triton kernels is listed in 3 for

Algorithm B VVOR Kernel for Computing Gradients $\nabla_{\mathbf{W}}$.

Inputs: Upstream gradients $\nabla \mathbf{F}^{\text{out}}, \mathbf{F}^{\text{in}}, \mathcal{T}^L$.

Output: Weight gradients $\nabla_{\mathbf{W}}$.

```
1:  $(\tilde{i}, \tilde{j}, \tilde{k}) \leftarrow \mathcal{T}_0^L$  ▷ initialize with the first triplet
2:  $\tilde{\mathbf{g}}_{\text{out}} \leftarrow \nabla \mathbf{F}_{\tilde{i}}^{\text{out}}, \tilde{\mathbf{f}}_{\text{in}} \leftarrow \mathbf{F}_{\tilde{j}}^{\text{in}}$  ▷ read from global memory
3:  $\nabla_{\tilde{\mathbf{W}}} \leftarrow \tilde{\mathbf{g}}_{\text{out}} \otimes \tilde{\mathbf{f}}_{\text{in}}$  ▷ fast on-chip computation

4: for all  $(i, j, k)$  in  $\mathcal{T}_{[1,2,\dots,L-1]}^L$  do
5:   if  $i \neq \tilde{i}$  then
6:      $\tilde{i} \leftarrow i, \tilde{\mathbf{g}}_{\text{out}} \leftarrow \nabla \mathbf{F}_i^{\text{out}}$  ▷ read only if necessary
7:   end if
8:   if  $j \neq \tilde{j}$  then
9:      $\tilde{j} \leftarrow j, \tilde{\mathbf{f}}_{\text{in}} \leftarrow \mathbf{F}_j^{\text{in}}$  ▷ read only if necessary
10:  end if

11:  if  $k \neq \tilde{k}$  then
12:    atomicAdd $(\nabla_{\mathbf{W}_{\tilde{k}}}, \nabla_{\tilde{\mathbf{W}}})$  ▷ only if necessary
13:     $\tilde{k} \leftarrow k, \nabla_{\tilde{\mathbf{W}}} \leftarrow \tilde{\mathbf{g}}_{\text{out}} \otimes \tilde{\mathbf{f}}_{\text{in}}$  ▷ on-chip, fast
14:  else ▷ on-chip, fast
15:     $\nabla_{\tilde{\mathbf{W}}} \leftarrow \nabla_{\tilde{\mathbf{W}}} + \tilde{\mathbf{g}}_{\text{out}} \otimes \tilde{\mathbf{f}}_{\text{in}}$ 
16:  end if
17: end for

18: atomicAdd $(\nabla_{\mathbf{W}_{\tilde{k}}}, \nabla_{\tilde{\mathbf{W}}})$ 
```

reference.

Listing 1. Triton implementation of MVMR kernel.

```

@triton.autotune(
    configs=[
        triton.Config(
            {
                "L": 128,
                "BLOCK_SIZE_G": 1,
                "BLOCK_SIZE_M": 32,
                "BLOCK_SIZE_C": 32,
            },
            num_warps=1,
        ),
    ],
    key=["T", "G", "M", "C"],
)
@triton.jit
def sparse_matrix_vector_multiplication_reduction_kernel(
    a, a_idx, b, b_idx, o, o_idx, T, G, M, C,
    L: tl.constexpr, BLOCK_SIZE_G: tl.constexpr,
    BLOCK_SIZE_M: tl.constexpr, BLOCK_SIZE_C: tl.constexpr,
):
    num_pid_g = tl.cdiv(G, BLOCK_SIZE_G)
    num_pid_m = tl.cdiv(M, BLOCK_SIZE_M)
    num_pid_c = tl.cdiv(C, BLOCK_SIZE_C)

    pid = tl.program_id(axis=0)
    pid_m = pid % num_pid_m
    pid //= num_pid_m
    pid_c = pid % num_pid_c
    pid //= num_pid_c
    pid_g = pid % num_pid_g
    pid_t = pid // num_pid_g

    g_offsets = pid_g * BLOCK_SIZE_G + tl.arange(0, BLOCK_SIZE_G)
    m_offsets = pid_m * BLOCK_SIZE_M + tl.arange(0, BLOCK_SIZE_M)
    c_offsets = pid_c * BLOCK_SIZE_C + tl.arange(0, BLOCK_SIZE_C)

    g_mask = g_offsets < G
    m_mask = m_offsets < M
    c_mask = c_offsets < C

    gm_mask = g_mask[:, None] & m_mask[None, :]
    gc_mask = g_mask[:, None] & c_mask[None, :]
    gcm_mask = g_mask[:, None, None] & c_mask[None, :, None] & m_mask[None, None, :]

    a_ptrs = a + (
        g_offsets[:, None, None] * (C * M)
        + c_offsets[None, :, None] * M
        + m_offsets[None, None, :]
    )
    b_ptrs = b + (g_offsets[:, None] * C + c_offsets[None, :])
    o_ptrs = o + (g_offsets[:, None] * M + m_offsets[None, :])

    t_offset = pid_t * L
    a_offset = tl.load(a_idx + t_offset)
    b_offset = tl.load(b_idx + t_offset)
    o_offset = tl.load(o_idx + t_offset)

    block_a = tl.load(a_ptrs + a_offset * (G * C * M), mask=gcm_mask)
    block_b = tl.load(b_ptrs + b_offset * (G * C), mask=gc_mask)
    block_o = tl.sum(block_a * block_b[:, :, None], axis=1)
    for t in tl.range(1, min(L, T - t_offset)):
        a_offset_next = tl.load(a_idx + t_offset + t)
        b_offset_next = tl.load(b_idx + t_offset + t)
        o_offset_next = tl.load(o_idx + t_offset + t)

        if a_offset_next != a_offset:
            block_a = tl.load(a_ptrs + a_offset_next * (G * C * M), mask=gcm_mask)
            a_offset = a_offset_next

        if b_offset_next != b_offset:
            block_b = tl.load(b_ptrs + b_offset_next * (G * C), mask=gc_mask)
            b_offset = b_offset_next

        if o_offset_next != o_offset:
            tl.atomic_add(o_ptrs + o_offset * (G * M), block_o, mask=gm_mask)
            o_offset = o_offset_next
            block_o = tl.sum(block_a * block_b[:, :, None], axis=1)
        else:
            block_o += tl.sum(block_a * block_b[:, :, None], axis=1)
    tl.atomic_add(o_ptrs + o_offset * (G * M), block_o, mask=gm_mask)

```

Listing 2. Triton implementation of VVOR kernel.

```

@triton.autotune(
    configs=[
        triton.Config(
            {
                "L": 128,
                "BLOCK_SIZE_G": 1,
                "BLOCK_SIZE_M": 32,
                "BLOCK_SIZE_C": 32,
            },
            num_warps=1,
        ),
    ],
    key=["T", "G", "M", "C"],
)
@triton.jit
def sparse_vector_vector_outer_product_reduction_kernel(
    a, a_idx, b, b_idx, o, o_idx, T, G, M, C,
    L: tl.constexpr, BLOCK_SIZE_G: tl.constexpr,
    BLOCK_SIZE_M: tl.constexpr, BLOCK_SIZE_C: tl.constexpr,
):
    num_pid_g = tl.cdiv(G, BLOCK_SIZE_G)
    num_pid_m = tl.cdiv(M, BLOCK_SIZE_M)
    num_pid_c = tl.cdiv(C, BLOCK_SIZE_C)

    pid = tl.program_id(axis=0)
    pid_c = pid % num_pid_c
    pid //= num_pid_c
    pid_m = pid % num_pid_m
    pid //= num_pid_m
    pid_g = pid % num_pid_g
    pid_t = pid // num_pid_g

    g_offsets = pid_g * BLOCK_SIZE_G + tl.arange(0, BLOCK_SIZE_G)
    m_offsets = pid_m * BLOCK_SIZE_M + tl.arange(0, BLOCK_SIZE_M)
    c_offsets = pid_c * BLOCK_SIZE_C + tl.arange(0, BLOCK_SIZE_C)

    g_mask = g_offsets < G
    m_mask = m_offsets < M
    c_mask = c_offsets < C

    gm_mask = g_mask[:, None] & m_mask[None, :]
    gc_mask = g_mask[:, None] & c_mask[None, :]
    gmc_mask = g_mask[:, None, None] & m_mask[None, :, None] & c_mask[None, None, :]

    a_ptrs = a + (g_offsets[:, None] * M + m_offsets[None, :])
    b_ptrs = b + (g_offsets[:, None] * C + c_offsets[None, :])
    o_ptrs = o + (
        g_offsets[:, None, None] * (M * C)
        + m_offsets[None, :, None] * C
        + c_offsets[None, None, :]
    )

    t_offset = pid_t * L
    a_offset = tl.load(a_idx + t_offset)
    b_offset = tl.load(b_idx + t_offset)
    o_offset = tl.load(o_idx + t_offset)

    block_a = tl.load(a_ptrs + a_offset * (G * M), mask=gm_mask)
    block_b = tl.load(b_ptrs + b_offset * (G * C), mask=gc_mask)
    block_o = block_a[:, :, None] * block_b[:, None, :]
    for t in tl.range(1, min(L, T - t_offset)):
        a_offset_next = tl.load(a_idx + t_offset + t)
        b_offset_next = tl.load(b_idx + t_offset + t)
        o_offset_next = tl.load(o_idx + t_offset + t)

        if a_offset_next != a_offset:
            block_a = tl.load(a_ptrs + a_offset_next * (G * M), mask=gm_mask)
            a_offset = a_offset_next

        if b_offset_next != b_offset:
            block_b = tl.load(b_ptrs + b_offset_next * (G * C), mask=gc_mask)
            b_offset = b_offset_next

        if o_offset_next != o_offset:
            tl.atomic_add(o_ptrs + o_offset * (G * M * C), block_o, mask=gmc_mask)
            o_offset = o_offset_next
            block_o = block_a[:, :, None] * block_b[:, None, :]
        else:
            block_o = tl.fma(block_a[:, :, None], block_b[:, None, :], block_o)
    tl.atomic_add(o_ptrs + o_offset * (G * M * C), block_o, mask=gmc_mask)

```

Listing 3. PyTorch code for invoking Triton MVMR and VVOR kernels.

```

def sparse_matrix_vector_multiplication_reduction(a, a_idx, b, b_idx, o_idx, n_o):
    assert a.is_cuda
    assert a_idx.is_cuda
    assert b.is_cuda
    assert b_idx.is_cuda
    assert o_idx.is_cuda

    a = a.contiguous()
    b = b.contiguous()

    T, G, M, C = a_idx.numel(), a.shape[1], a.shape[3], a.shape[2]
    o = torch.zeros((n_o, G, M), dtype=a.dtype, device=a.device)

    grid = lambda META: (
        triton.cdiv(T, META["L"])
        * triton.cdiv(G, META["BLOCK_SIZE_G"])
        * triton.cdiv(M, META["BLOCK_SIZE_M"])
        * triton.cdiv(C, META["BLOCK_SIZE_C"]),
    )
    sparse_matrix_vector_multiplication_reduction_kernel[grid](a, a_idx, b, b_idx, o, o_idx, T, G, M, C)

    return o

def sparse_vector_vector_outer_product_reduction(a, a_idx, b, b_idx, o_idx, n_o):
    assert a.is_cuda
    assert a_idx.is_cuda
    assert b.is_cuda
    assert b_idx.is_cuda
    assert o_idx.is_cuda

    a = a.contiguous()
    b = b.contiguous()

    T, G, M, C = a_idx.numel(), a.shape[1], a.shape[2], b.shape[2]
    o = torch.zeros((n_o, G, M, C), dtype=a.dtype, device=a.device)

    grid = lambda META: (
        triton.cdiv(T, META["L"])
        * triton.cdiv(G, META["BLOCK_SIZE_G"])
        * triton.cdiv(M, META["BLOCK_SIZE_M"])
        * triton.cdiv(C, META["BLOCK_SIZE_C"]),
    )
    sparse_vector_vector_outer_product_reduction_kernel[grid](a, a_idx, b, b_idx, o, o_idx, T, G, M, C)

    return o

```